First-principles study of structural, magnetic, and electronic properties of small Fe-Rh alloy clusters

Junais Habeeb Mokkath and G. M. Pastor
Institut für Theoretische Physik, Universität Kassel, Heinrich Plett Straße 40, DE-34132 Kassel, Germany
(Received 24 June 2011; revised manuscript received 24 January 2012; published 7 February 2012)

The structural, electronic, and magnetic properties of small Fe_mRh_n clusters having $N = m + n \leqslant 8$ atoms are studied in the framework of a generalized-gradient approximation to density-functional theory. For $N = m + n \leqslant 6$, a thorough sampling of all cluster topologies has been performed, while for $N = 7$ and 8, only a few representative topologies are considered. In all cases, the entire concentration range is systematically investigated. All the clusters show ferromagnetic-like order in the optimized structures. As a result, the average magnetic moment per atom $\overline{\mu}_N$ increases monotonously, which is almost linear over a wide range of concentration with Fe content. A remarkable enhancement of the local Fe moments beyond $3\mu_B$ is observed as result of Rh doping. The composition dependence of the binding energy, average magnetic moment, and electronic structure are discussed.

DOI: 10.1103/PhysRevB.85.054407 PACS number(s): 75.75.−c, 36.40.Cg, 75.50.Bb, 73.22.−f

I. INTRODUCTION

Alloying elements with complementary qualities in order to tailor their physical behavior for specific technological purposes has been a major route in material development since the antiquity. Cluster research is no exception to this trend. After decades of systematic studies of the size and structural dependence of the most wide variety of properties of monoelement particles, the interest has actually been moving progressively over the past years toward investigations on finite-size binary alloys.[1] The magnetism of transition-metal (TM) clusters opens numerous possibilities and challenges in this context.[2–17] For example, one would like to understand how to modify the magnetic characteristics of clusters, in particular, the saturation magnetization and the magnetic anisotropy energy (MAE), as it has been done in solids. This would indeed allow one to design new nanostructured materials from a microscopic perspective. Nevertheless, it is also true that controlling composition, system size, and magnetic behavior sets serious difficulties for both experiment and theory.

Pure TM clusters such as Fe_N, Co_N, and Ni_N show spin moments, orbital moments, and MAEs that are enhanced with respect to the corresponding periodic solids.[18–24] Still, the possibilities of optimizing the cluster magnetic behavior by simply tuning the system size have been rather disappointing, particularly concerning the MAE, which remains relatively small—despite being orders of magnitude larger than in solids[21]—due to the rather weak spin-orbit (SO) coupling in the 3*d* atoms. This is one of the motivations for alloying 3*d* TMs with 4*d* and 5*d* elements which, being heavier, are subject to stronger SO interactions. In this context, it is useful to recall that large nanoparticles and three-dimensional solids of these elements are nonmagnetic. However, at very small sizes, the 4*d* and 5*d* clusters often develop a finite spontaneous low-temperature magnetization due to the reduction of local coordination and the resulting *d*-band narrowing.[25–29] The first experimental observation of this important finite-size effect has been made by Cox *et al.* by performing Stern-Gerlach-deflection measurements on Rh_N clusters. In this work, the average magnetic moments per atom $\overline{\mu}_N = 0.15$–$0.80\mu_B$ have been experimentally determined for $N \leqslant 30$–50 atoms.[27] In view of these contrasting features, one expects that 3*d*-4*d* and 3*d*-5*d* alloy clusters should show very interesting structural, electronic, and magnetic behaviors.

The purpose of this paper is to investigate the ground-state properties of the small FeRh clusters in the framework of Hohenberg-Kohn-Sham's density functional theory.[30] Besides the general interest of the problem from the perspective of 3*d*-4*d* nanomagnetism, these clusters are particularly appealing because of the remarkable phase diagram of FeRh bulk alloys.[31] In the case of $Fe_{50}Rh_{50}$, the magnetic order at normal pressure and low temperatures is antiferromagnetic (AF). As the temperature increases, this α'' phase undergoes a first-order transition to a ferromagnetic (FM) state, the α' phase, which is accompanied by a change in lattice parameter. The corresponding transition temperature $T_c^{\alpha'\alpha''}$ increases rapidly with increasing external pressure P, eventually displacing the FM α' phase completely for $P \geqslant 7$ GPa ($T_c^{\alpha'\alpha''} \simeq 290K$ for $Fe_{50}Rh_{50}$ at normal pressure). Moreover, $T_c^{\alpha'\alpha''}$ decreases very rapidly with decreasing Rh content. At low pressures the FM α' phase undergoes a FM to paramagnetic (PM) transition at ($T_C \simeq 670K$).[31] In addition, the properties of α-FeRh bulk alloys have been the subject of first-principles and model theoretical investigations.[32] In particular, these show that the relative stability of the FM and AF solutions depends strongly on the interatomic distances. Such remarkable condensed-matter effects enhance the appeal of small FeRh particles as specific example of 3*d*-4*d* nanoscale alloy. Investigations of their magnetic properties as a function of size, composition, and structure are therefore of fundamental importance.

The remainder of the paper is organized as follows. In Sec. II, the main details of the theoretical background and computational procedure are presented. This includes, in particular, a description of the strategy used for exploring the cluster energy landscape as a function of geometrical conformation and chemical order. The results of our calculations for FeRh clusters having $N \leqslant 8$ atoms are reported in Sec. III by analyzing the concentration dependence of the cohesive energy, the local and average magnetic moments, and the spin-polarized electronic structure. Finally, we conclude in Sec. IV with a summary of the main trends and an outlook to future extensions.

II. COMPUTATIONAL ASPECTS

The calculations reported in this work are based on density functional theory,[30] as implemented in the Vienna *ab initio* simulation package (VASP).[33] The exchange and correlation energy is described by using both the spin-polarized local density approximation (LDA) and Perdew and Wang's generalized-gradient approximation (GGA).[34] The VASP solves the spin-polarized Kohn-Sham equations in an augmented plane-wave basis set, taking into account the core electrons within the projector augmented wave (PAW) method.[35] This is an efficient frozen-core all-electron approach that allows to incorporate the proper nodes of the Kohn-Sham orbitals in the core region and the resulting effects on the electronic structure, total energy, and interatomic forces. The 4*s* and 3*d* orbitals of Fe and the 5*s* and 4*d* orbitals of Rh are treated as valence states. The wave functions are expanded in a plane-wave basis set with the kinetic energy cutoff $E_{\max} = 268$ eV. In order to improve the convergence of the solution of the self-consistent KS equations, the discrete energy levels are broadened by using a Gaussian smearing $\sigma = 0.02$ eV. The validity of the present choice of computational parameters has been verified.[36] The PAW sphere radii for Fe and Rh are 1.302 and 1.402 Å, respectively. A simple cubic supercell is considered with the usual periodic boundary conditions. The linear size of the cell is $a = 10$–22 Å, so that any pair of images of the clusters are well separated and the interaction between them is negligible. Since we are interested in finite systems, the reciprocal space summations are restricted to the Γ point.

Although the potential advantages of alloying magnetic 3*d* elements with highly polarizable 4*d* or 5*d* elements are easy to understand, the problem involves a number of serious practical challenges. Different growth or synthesis conditions can lead to different chemical orders, which can be governed not just by energetic reasons but by kinetic processes as well. For instance, one may have to deal with segregated clusters having either a 4*d* core and a 3*d* outer shell or vice versa. Postsynthesis manipulations can induce different degrees of intermixing, including, for example, surface diffusion or disordered alloys. Moreover, the interatomic distances are also expected to depend strongly on size and composition. Typical TM-cluster bond lengths are in fact 10–20% smaller than in the corresponding bulk crystals. Taking into account that itinerant 3*d*-electron magnetism is most sensitive to the local and chemical environments of the atoms,[26,37–39] it is clear that controlling the distribution of the elements within the cluster is crucial for understanding magnetic nanoalloys.

Systematic theoretical studies of binary-metal clusters are hindered by the diversity of geometrical conformations, ordered and disorder arrangements as well as segregation tendencies that have to be taken into account. This poses a serious challenge to both first-principles and model approaches. In order to determine the interplay between cluster structure, chemical order, and magnetism in FeRh clusters, we have performed a comprehensive set of electronic calculations for clusters having $N \leqslant 8$ atoms. In the present paper, we focus on the most stable cluster structure and magnetic configuration, which are determined by exploring the ground-state energy landscape.[40] This is a formidable task, since one needs to consider a large, most possibly complete and unbiased set of initial structures. Such a thorough geometry optimization must include not only the representative cluster geometries or topologies, but also all relevant chemical orders. This requires taking into account all distributions of the Fe and Rh atoms for any given size and composition. These two aspects of the problem of determining the structure of nanoalloys are discussed in more detail in the following.

The different cluster topologies are sampled by generating all possible graphs for $N \leqslant 6$ atoms as described in Ref. 38 (see also Ref. 41). For each graph or adjacency matrix, it is important to verify that it can be represented by a true structure in $D \leqslant 3$ dimensions. A graph is acceptable as a cluster structure, only if a set of atomic coordinates $\vec{R}_i$ with $i = 1, \ldots, N$ exists, such that the interatomic distances R_{ij} satisfy the conditions $R_{ij} = R_0$ if the sites i and j are connected in the graph (i.e., if the adjacency matrix element $A_{ij} = 1$) and $R_{ij} > R_0$ otherwise (i.e., if $A_{ij} = 0$). Here, R_0 refers to the nearest-neighbor (NN) distance, which at this stage can be regarded as the unit of length, assuming for simplicity that it is the same for all clusters. Notice that for $N \leqslant 4$ all graphs are possible cluster structures. For example, for $N = 4$, the different structures are the tetrahedron, rhombus, square, star, triangular racket and linear chain.[38] However, for $N \geqslant 5$, there are graphs, i.e., topologies, which cannot be realized in practice. For instance, it is not possible to have five atoms being NNs from each other in a three-dimensional space. Consequently, for $N \geqslant 5$, there are less real structures than mathematical graphs. The total number of graphs (structures) is 21 (20), 112 (104), and 853 (647) for $N = 5$,6, and 7, respectively.[38]

For clusters having $N \leqslant 6$ atoms, all these topologies have indeed been taken as starting points of our structural relaxations. Out of this large number of different initial configurations the unconstrained relaxations using VASP lead to only a few geometries, which can be regarded as stable or metastable isomers. For larger clusters ($N = 7$ and 8), we do not aim at performing a full global optimization. Our purpose here is to explore the interplay between magnetism and chemical order as a function of composition for a few topologies that are representative of open and close-packed structures. Taking into account our results for smaller sizes, and the available information on the structure of pure Fe_N and Rh_N clusters, we have restricted the set of starting topologies for the unconstrained relaxation of FeRh heptamers and octamers to the following: bicapped trigonal bipyramid, capped octahedra, and pentagonal bipyramid for $N = 7$, and tricapped trigonal bipyramid, bicapped octahedra, capped pentagonal bipyramid and cube for $N = 8$. Although, the choice of topologies for $N = 7$ and 8 is quite restricted, it includes compact as well as more open structures. Therefore, it is expected to shed light on the dependence of the magnetic properties on the chemical order and composition.

The dependence on concentration is investigated systematically for each topology of Fe_mRh_n by varying m and for each size $N = m + n \leqslant 8$, including the pure Fe_N and Rh_N limits. Moreover, we take into account all possible nonequivalent distributions of the m Fe and n Rh atoms within the cluster. In this way, any *a priori* assumption on the chemical order is avoided. Obviously, such an exhaustive combinatorial search

increasingly complicates the computational task as we increase the cluster size, and as we move away from pure clusters toward alloys with equal concentrations. Finally, in order to perform the actual density-functional calculations, we set for simplicity all NN distances in the starting cluster geometry equal to the Fe bulk value[42] $R_0 = 2.48$ Å. Subsequently, a fully unconstrained geometry optimization is performed from first principles by using the VASP.[33] The atomic positions are fully relaxed by means of conjugate gradient or quasi-Newtonian methods, without imposing any symmetry constraints, until all the force components are smaller than the threshold 5 meV/Å. The convergence criteria are set to 10^{-5} eV/Å for the energy gradient, and 5×10^{-4} Å for the atomic displacements.[43] The same procedure applies to all considered clusters regardless of composition, chemical order, or total magnetic moment. Notice that the diversity of geometrical structures and atomic arrangements often yields many local minima on the ground-state energy surface, which complicates significantly the location of the lowest-energy configuration.

Lattice structure and magnetic behavior are intimately related in TMs, particularly in weak ferromagnets such as Fe and its alloys.[44] On the one side, the optimum structure and chemical order depend on the actual magnetic state of the cluster as given by the average magnetic moment per atom $\overline{\mu}_N$ and the magnetic order. On the other side, the magnetic behavior is known to be different for different structures and concentrations. Therefore, in order to rigorously determine the ground-state magnetic properties of FeRh clusters, we have varied systematically the value of the total spin polarization of the cluster S_z by performing fixed spin-moment (FSM) calculations in the whole physically relevant range. Let us recall that $S_z = (\nu_\uparrow - \nu_\downarrow)/2$, where $\nu_\uparrow(\nu_\downarrow)$ represents the number of electrons in the majority (minority) states. In practice, we start from the nonmagnetic state ($S_z^{\min} = 0$) and increase S_z until the local spin moments are fully saturated, i.e., until the Fe moments in the PAW sphere reach $\mu_{\mathrm{Fe}} \simeq 4\mu_B$ and the Rh moments $\mu_{\mathrm{Rh}} \simeq 2.5\mu_B$ (typically, $S_z^{\max} \gtrsim 3N/2$). The above described global geometry optimizations are performed independently for each value of S_z. These FSM study provides a wealth of information on the isomerization energies, the spin-excitation energies, and their interplay. These are particularly interesting for a subtle magnetic alloy such as FeRh, and would therefore deserve to be analyzed in some more detail. In the present paper, we shall focus on the ground-state properties by determining for each considered $\mathrm{Fe}_m\mathrm{Rh}_n$ the most stable structural and magnetic configuration corresponding to energy minimum as a function of S_z and of the atomic positions.[40]

Once the optimization with respect to structural and magnetic degrees of freedom is achieved, we derive the binding energy per atom $E_B = [mE(\mathrm{Fe}) + nE(\mathrm{Rh}) - E(\mathrm{Fe}_m\mathrm{Rh}_n)]/N$ in the usual way by referring the total energy E to the corresponding energy of m Fe and n Rh isolated atoms. Moreover, for each stationary point of the total energy surface (i.e., for each relaxed structure having a nearly vanishing $\|\vec{\nabla}E\|$) we determine the vibrational frequencies from the diagonalization of the dynamical matrix. The latter is calculated from finite differences of the analytic gradients of the total energy. In this way, we can rule out saddle points to which the local optimization procedure happens to converge on some occasions. Only configurations that correspond to true minima are discussed in the following. Finally, a number of electronic and magnetic properties—for example, the binding energy, the local magnetic moments μ_i integrated within the Wigner-Seitz (WS) or Bader atomic cells of atom i,[45,46] and the spin polarized density of electronic states (DOS) $\rho_\sigma(\varepsilon)$—are derived from the self-consistent spin-polarized density and Kohn-Sham spectrum.

III. RESULTS AND DISCUSSION

In the following, we present and discuss results for the binding energy, average and local spin moments, and electronic densities of states for $N = m + n \leqslant 8$.

A. Binding energy and magnetic moments

In Fig. 1, the binding energy per atom E_B is given as a function of the number of Fe atoms m. Besides the expected monotonic increase of E_B with increasing N, an interesting concentration dependence is observed. For very small sizes ($N \leqslant 4$), E_B is maximal for $m = 1$ or 2, despite the fact that E_B is always larger for pure Rh than pure Fe clusters. This indicates that in these cases the bonding resulting from FeRh pairs is stronger than RhRh bonds. Only for $m \geqslant N - 1$, when the number of weaker FeFe bonds dominates, one observes that E_B decreases with increasing m. For larger sizes ($N \geqslant 5$), the strength of RhRh and FeRh bonds becomes very similar, so that the maximum in E_B is replaced by a range of Fe concentrations $x = m/N \lesssim 0.5$ where E_B depends very weakly on m.

In Fig. 2, the average magnetic moments $\overline{\mu}_N$ of $\mathrm{Fe}_m\mathrm{Rh}_n$ are shown as a function of m for $N \leqslant 8$. First of all, one observes that $\overline{\mu}_N$ increases monotonously, with the number of Fe atoms. This is an expected consequence of the larger Fe local moments and the underlying FM-like magnetic order. The average slope of the curves tends to increase with decreasing N, since the change in concentration per Fe substitution is more important the smaller the size is. The typical increase in $\overline{\mu}_N$ per Fe substitution is about $(1/N)\mu_B$ per Fe substitution. Notice, moreover, the enhancement of the magnetic moments of the pure clusters in particular for Fe_N ($m = N$), which go well beyond $3\mu_B$, the value corresponding to a saturated d-band in the d^7s^1 configuration. In contrast, the moments of pure Rh_N are far from saturated except for $N = 2$ and 7 (see Fig. 2 for $m = 0$). In this context, it is important to recall that a

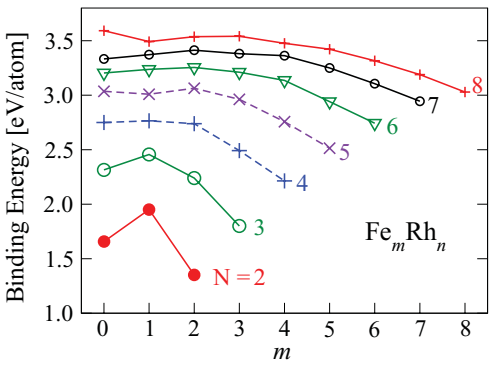

FIG. 1. (Color online) Binding energy per atom E_B of $\mathrm{Fe}_m\mathrm{Rh}_n$ clusters as a function of the number of Fe atoms. The lines connecting the points for each $N = m + n$ are a guide to the eye.

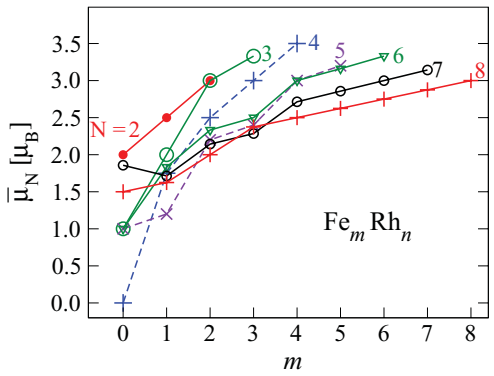

FIG. 2. (Color online) Total magnetic moment per atom $\overline{\mu}_N$ of Fe_mRh_n clusters as a function of number of Fe atoms. The symbols corresponding to each size are the same as in Fig. 1. The lines connecting the points for each $N = m + n$ are a guide to the eye.

thorough global optimization, for example, by considering a large number of initial topologies, could affect the quantitative values of the magnetic moments for $N = 7$ and 8.

The local magnetic moments in the PAW sphere of the Fe and Rh atoms provide further insight on the interplay between $3d$ and $4d$ magnetism in Fe_mRh_n. In Fig. 3, μ_{Fe} and μ_{Rh} are shown as a function of m for $N = 6$–8. The Fe moments are essentially given by the saturated d-orbital contribution. For pure Fe clusters, the actual values of μ_{Fe} within the PAW sphere are somewhat lower than $3\mu_B$ due to a partial spill-off of the spin-polarized density. Notice that the Fe moments increase as we replace Fe by Rh atoms showing some weak oscillations as a function of m. The increase is rather weak for a single Rh impurity in $Fe_{N-1}Rh$ but becomes stronger reaching a more or less constant value as soon as the cluster contains 2 or more Rh ($m \leqslant N - 2$, see Fig. 3). This effect can be traced back to a d electron charge transfer from Fe to Rh which, together with the extremely low coordination number, yields a full polarization of the larger number of Fe d holes. On the other side, the Rh moments are not saturated and therefore are more sensitive to size, structure, and composition. The values of μ_{Rh} are in the range of 1–1.5μ_B showing some oscillations as a function of m. No systematic enhancement of μ_{Rh} with increasing Fe content is observed. This behavior could be related to charge transfers effects leading to changes in the number of Rh d electrons as a function of m.

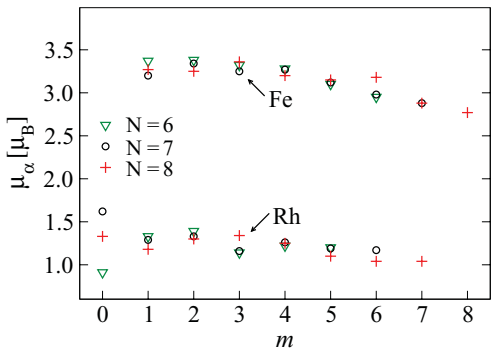

FIG. 3. (Color online) Local magnetic moment μ_α at the Fe and Rh atoms as a function of the number Fe atoms m.

Finally, it is interesting to analyze the role played by magnetism in defining the cluster structure by comparing magnetic and nonmagnetic calculations. For the smallest FeRh clusters ($N = 3$ and 4), the magnetic energy $\Delta E_m = E(S_z = 0) - E(S_Z)$ gained upon magnetization is higher in the first excited isomer than in the most stable structure. This implies that the contribution of magnetism to the structural stability is not crucial, since the nonmagnetic calculations yield the same ordering, at least concerning the two best structures. This suggests that for the smallest sizes the kinetic or bonding energy dominates the structural stability, which also explains that the two most stable isomers have different topologies. The situation changes for large clusters. For $N \geqslant 5$, one finds a number of FeRh clusters for which the optimal structure is actually stabilized by magnetism. For example, in Fe_4Rh, Fe_3Rh_2, and $FeRh_4$ the energy ordering of the two most stable isomers would be reversed if magnetism were neglected. It should be noted that in these cases, the structures differ only in the chemical order, not in the topology which is a trigonal bipyramid. In the FeRh hexamers, the energy differences between the low-lying isomers are more important and only in one case, Fe_4Rh_2, magnetism appears to be crucial for stabilizing the actual optimal structure. A similar strong interplay between structure, chemical order, and magnetism is expected for larger FeRh clusters.

B. Electronic structure

It is very interesting to analyze, at least for some representative examples, how the electronic structure depends on the composition of magnetic nanoalloys. To this aim we report in Fig. 4 the spin-polarized d-electron density of states (DOS) of representative FeRh octamers having the most stable relaxed configuration among the considered topologies (see Sec. II). Results for pure Fe_8 and Rh_8 are also shown for the sake of comparison. In all the clusters, the dominant peaks in the relevant energy range near ε_F correspond either to the Fe-$3d$ or to the Rh-$4d$ states. The valence spectrum is largely dominated by these d-electron contributions. In fact, the total DOS and the d-projected DOS are difficult to tell apart.

First of all, let us consider the DOS of the pure clusters. Our results for Rh_8 with a cube structure are similar to those of previous studies.[47] They show the dominant d-electron contribution near ε_F, with the characteristic ferromagnetic exchange splitting between the minority- and majority-spin states. In Fig. 4, we also included the DOS for Rh_8 with a bicapped octahedron (BCO) structure, since it allows us to illustrate the differences in the electronic structure of compact and open geometries. Moreover, the DOS of pure Rh_8 with BCO structure is very useful in order to demonstrate the dependence of DOS on Fe content, since the structures of Fe_mRh_{8-m} with $m \geqslant 1$ are similar to the BCO. Both Fe_8 and Rh_8 show relatively narrow d bands, which dominate the single-particle energy spectrum in the range $-5\text{eV} \leqslant \varepsilon - \varepsilon_F \leqslant 3\text{eV}$. The spin polarization of the DOS clearly reflects the ferromagnetic order in the cluster. Putting aside the exchange splitting, the peak structure in the up and down DOS $\rho_\sigma(\varepsilon)$ are comparable. There are even qualitative similarities between the two elements. However, looking in more detail, one observes that the effective d-band width in

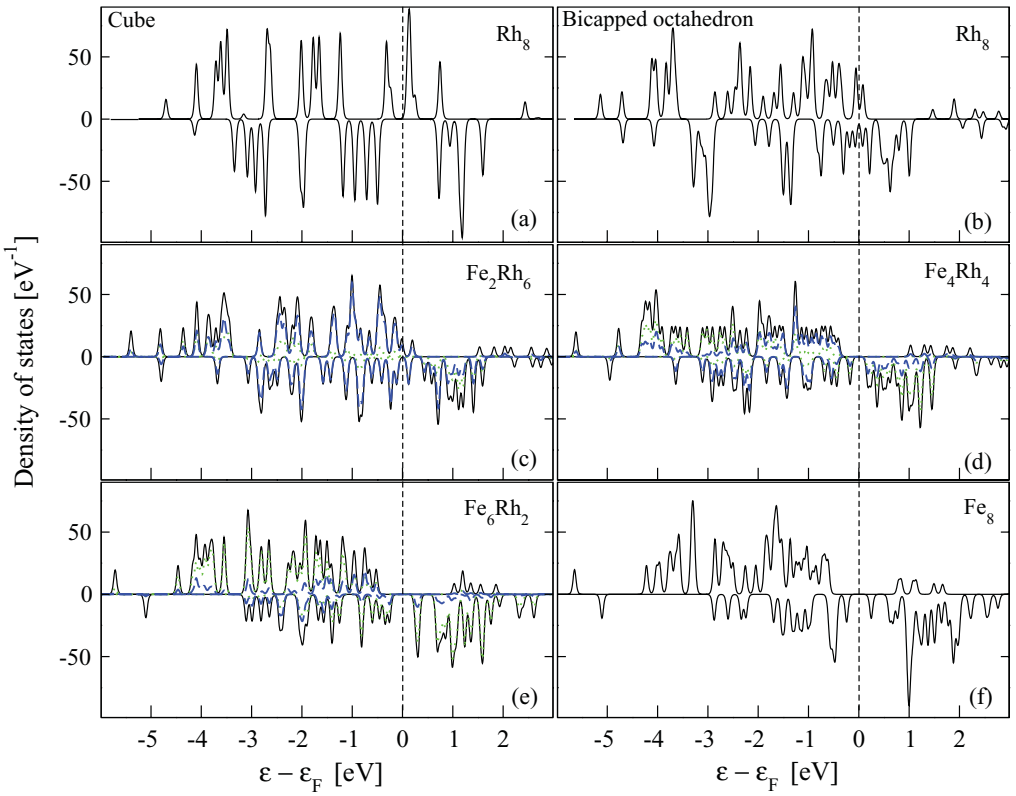

FIG. 4. (Color online) Electronic density of states (DOS) of FeRh octamers. Results are given for the total (solid), the Fe-projected (dotted), and the Rh-projected (dashed) d-electron DOS. Positive (negative) values correspond to majority (minority) spin. A Lorentzian width $\lambda = 0.02$ eV has been used to broaden the discrete energy levels.

Fe_8 (about 4 eV) is somewhat smaller than in Rh_8 (about 5 eV). Moreover, in Rh_8 the DOS at ε_F is nonvanishing for both spin directions and the finite-size gaps are very small (see Fig. 4). In contrast, the majority d-DOS is fully occupied in Fe_8, with the highest majority state lying about 0.5 eV below ε_F. In addition, there is an appreciable gap (about 0.1 eV) in the corresponding minority spectrum. These qualitative differences are of course consistent with the fact that Fe_8 is a strong ferromagnet with saturated moments, while Rh_8 should be regarded as a weak unsaturated ferromagnet.

The trends as a function of concentration reflect the crossover between the previous contrasting behaviors. For low Fe concentration (e.g., Fe_2Rh_6), we still find states with both spin directions close to ε_F. The magnetic moments are not saturated, although the Fermi energy tends to approach the top of the majority band. Moreover, the majority-spin states close to ε_F have dominantly Rh character. Small Fe doping does not reduce the d-band width significantly. Notice the rather important change in the shape of the DOS in Fe_2Rh_6 as compared to the DOS in Rh_8. This is a consequence of the change in topology from cubic to bicapped octahedron (BCO).

For equal concentrations (Fe_4Rh_4), the first signs of d-band narrowing and enhanced exchange splitting start to become apparent. The spin-up states (majority band), which in Fe_2Rh_6 contribute to the DOS at ε_F now move to lower energies (0.3 eV below ε_F) so that the majority band is saturated. Only spin-down (minority) states are found around ε_F, although there is a significant gap in $\rho_\downarrow(\varepsilon)$ (see Fig. 4). In the majority band, Rh dominates over Fe at the higher energies (closer to ε_F), while Fe dominates in the bottom of the band. In the minority band, the participation of Rh (Fe) is stronger (weaker) below ε_F and weaker (stronger) above ε_F. This is consistent with the fact that the Rh local moments are smaller than the Fe moments.

Finally, in the Fe-rich limit (e.g., Fe_6Rh_2), the majority-band width becomes as narrow as in Fe_8, while the minority band is still comparable to Rh_8. The exchange splitting is large, the majority band saturated and only minority states are found close to ε_F. As in Fe_8, $\rho_\downarrow(\varepsilon)$ shows a clear gap at ε_F (see Fig. 4). However, the Rh contribution to the minority states below ε_F remains above average despite the relative small Rh content. The Fe contribution largely dominates the unoccupied minority-spin DOS, in agreement with the larger local Fe moments.

IV. SUMMARY AND OUTLOOK

The structural, electronic, and magnetic properties of small Fe_mRh_n clusters having $N = m + n \leqslant 8$ atoms have been investigated systematically in the framework of a generalized gradient approximation to density-functional theory. For very small sizes ($N \leqslant 4$ atoms), the binding energy E_B shows a nonmonotonous dependence on concentration, which implies that the FeRh bonds are stronger than the homogeneous ones. However, for larger sizes, the FeRh and RhRh bond strengths become comparable, so that E_B depends weakly on concentration for high Rh content.

The magnetic order of the clusters having the most stable structures is found to be FM-like. Moreover, the average

magnetic moment per atom $\overline{\mu}_N$ increases monotonously, which is almost linear over a wide range of concentration with Fe content. Consequently, the energy gain ΔE_m associated to magnetism also increases with the number of Fe atoms. The largest part of the spin polarization (about 90%) can be traced back to the local d magnetic moments within the PAW sphere of the atoms. The s and p spin polarizations are almost negligible in general. A remarkable enhancement of the local Fe moments is observed as a result of Rh doping. This is a consequence of the increase in the number of Fe d holes, due to charge transfer from Fe to Rh, combined with the extremely reduced local coordination. The Rh local moments are important already in the pure clusters ($N \leqslant 8$). Therefore they are not significantly enhanced by Fe doping. However, the overall stability of magnetism, as measured by the total energy gained by the onset of spin polarization, is found to increase with increasing Fe content.

FeRh clusters are expected to develop a variety of further interesting behaviors, which still remain to be explored. For instance, larger cluster should show a more complex dependence of the magnetic order as a function of concentration. In particular, for large Rh content, one should observe a transition from FM-like to AF-like order with increasing cluster size, in agreement with the AF phase found in solids for more than 50% Rh concentration. Moreover, the metamagnetic transition observed in bulk FeRh alloys also puts forward the possibility of similar interesting phenomena in nanoalloys as a function of temperature. Finally, the contributions of orbital magnetism and magnetic anisotropy deserve to be explored in detail as a function of composition and chemical order, even for the smallest sizes, particularly because of their implications for potential applications.[48]

ACKNOWLEDGMENTS

It is pleasure to thank Dr. J. L. Ricardo-Chávez and Dr. L. Díaz-Sánchez for helpful discussions and useful comments. Computer resources provided by ITS (Kassel) and CSC (Frankfurt) are gratefully acknowledged.

[1] See, for instance, *Nanoalloys: From Theory to Applications*, edited by R. L. Johnston and R. Ferrando, Faraday Discuss. **138**, 1 (2008).
[2] D. Zitoun, M. Respaud, M.-C. Fromen, M. J. Casanove, P. Lecante, C. Amiens, and B. Chaudret, Phys. Rev. Lett. **89**, 037203 (2002).
[3] S. Dennler, J. L. Ricardo-Chávez, J. Morillo, and G. M. Pastor, Eur. Phys. J. D **24**, 237 (2003).
[4] I. Efremenko and M. Sheintuch, Chem. Phys. Lett. **401**, 232 (2005).
[5] S. Ganguly, M. Kabir, S. Datta, B. Sanyal, and A. Mookerjee, Phys. Rev. B **78**, 014402 (2008).
[6] P. Entel and M. E. Gruner, J. Phys. Condens. Matter **21**, 064228 (2009).
[7] A. N. Andriotis, G. Mpourmpakis, G. E. Froudakis, and M. Menon, J. Chem. Phys. **120**, 11901 (2004).
[8] G. Rollmann, S. Sahoo, A. Hucht, and P. Entel, Phys. Rev. B **78**, 134404 (2008).
[9] J. Bansmann, S. Baker, C. Binns, J. Blackman, J.-P. Buecher, J. Dorantes-Dávila, V. Dupuis, L. Favre, D. Kechrakos, A. Kleibert, K.-H. Meiwes-Broer, G. M. Pastor, A. Perez, O. Toulemonde, K. N. Trohidou, J. Tuaillon, and Y. Xie, Surf. Sci. Rep. **56**, 189 (2005).
[10] C. Antoniak, J. Lindner, M. Spasova, D. Sudfeld, M. Acet, M. Farle, K. Fauth, U. Wiedwald, H.-G. Boyen, P. Ziemann, F. Wilhelm, A. Rogalev, and S. Sun, Phys. Rev. Lett. **97**, 117201 (2006).
[11] S. Yin, R. Moro, X. Xu, and W. A. de Heer, Phys. Rev. Lett. **98**, 113401 (2007).
[12] M. B. Knickelbein, Phys. Rev. B **75**, 014401 (2007).
[13] R. M. Wang, O. Dmitrieva, M. Farle, G. Dumpich, H. Q. Ye, H. Poppa, R. Kilaas, and C. Kisielowski, Phys. Rev. Lett. **100**, 017205 (2008).
[14] M. E. Gruner, G. Rollmann, P. Entel, and M. Farle, Phys. Rev. Lett. **100**, 087203 (2008).
[15] Yan Sun, Min Zhang, and René Fournier, Phys. Rev. B **77**, 075435 (2008).
[16] Yan Sun, René Fournier, and Min Zhang, Phys. Rev. A **79**, 043202 (2009).
[17] F. Tournus, A. Tamion, N. Blanc, A. Hannour, L. Bardotti, B. Prével, P. Ohresser, E. Bonet, T. Epicier, and V. Dupuis, Phys. Rev. B **77**, 144411 (2008).
[18] G. M. Pastor, J. Dorantes-Dávila, and K. H. Bennemann, Physica B **149**, 22 (1988); Phys. Rev. B **40**, 7642 (1989).
[19] J. P. Bucher, D. C. Douglass, and L. A. Bloomfield, Phys. Rev. Lett. **66**, 3052 (1991); D. C. Douglass, J. P. Bucher, and L. A. Bloomfield, Phys. Rev. B **45**, 6341 (1992); D. C. Douglass, A. J. Cox, J. P. Bucher, and L. A. Bloomfield, *ibid.* **47**, 12874 (1993).
[20] I. M. L. Billas, J. A. Becker, A. ChaËtelain, and W. A. de Heer, Phys. Rev. Lett. **71**, 4067 (1993); I. M. L. Billas, A. Châtelain, and W. A. de Heer, Science **265**, 1682 (1994).
[21] G. M. Pastor, J. Dorantes-Dávila, S. Pick, and H. Dreyssé, Phys. Rev. Lett. **75**, 326 (1995).
[22] S. E. Apsel, J. W. Emmert, J. Deng, and L. A. Bloomfield, Phys. Rev. Lett. **76**, 1441 (1996).
[23] M. B. Knickelbein, Phys. Rev. Lett. **86**, 5255 (2001).
[24] G. Nicolas, J. Dorantes-Dávila, and G. M. Pastor, Phys. Rev. B **74**, 014415 (2006).
[25] R. Galicia, Rev. Mex. Fis. **32**, 51 (1985).
[26] J. Dorantes-Dávila, H. Dreyssé, and G. M. Pastor, Phys. Rev. B **46**, 10432 (1992).
[27] A. J. Cox, J. G. Louderback, and L. A. Bloomfield, Phys. Rev. Lett. **71**, 923 (1993); A. J. Cox, J. G. Louderback, S. E. Apsel, and L. A. Bloomfield, Phys. Rev. B **49**, 12295 (1994).
[28] B. V. Reddy, S. N. Khanna, and B. I. Dunlap, Phys. Rev. Lett. **70**, 3323 (1993).
[29] P. Villaseñor-González, J. Dorantes-Dávila, H. Dreyssé, and G. M. Pastor, Phys. Rev. B **55**, 15084 (1997).
[30] P. Hohenberg and W. Kohn, Phys. Rev. **136**, B864 (1964); W. Kohn and L. J. Sham, *ibid.* **140**, A1133 (1965).
[31] T. B. Massalski, J. L. Murray, L. H. Bennett, and H. Baker, *Binary Alloy Phase Diagrams*, (American Society for Metals, Metals Park, OH, 1986), Vol. 1.

[32]M. E. Gruner, E. Hoffmann, and P. Entel, Phys. Rev. B **67**, 064415 (2003).

[33]G. Kresse and J. Furthmüller, Phys. Rev. B **54**, 11169 (1996); G. Kresse and D. Joubert, *ibid.* **59**, 1758 (1999).

[34]J. P. Perdew, J. A. Chevary, S. H. Vosko, K. A. Jackson, M. R. Pederson, D. J. Singh, and Carlos Fiolhais, Phys. Rev. B **46**, 6671 (1992).

[35]P. E. Blöchl, Phys. Rev. B **50**, 17953 (1994).

[36]A number of tests have been performed in order to assess the numerical accuracy of the calculations. Increasing the cutoff energy $E_{\max} = 268$ eV and supercell size $a = 12$ Å to $E_{\max} = 500$ eV and $a = 22$ Å in Rh_4 increases the computation time by a factor 4–7. This yields a total energy differences of 1.75 and 0.25 meV, respectively. In the above calculations, the change in average bond length (bond angle) amounts to 10^{-3} Å (10^{-4} degrees). These differences are not significant for our physical conclusions. In fact, typical isomerization energies in these clusters are an order of magnitude larger, of the order of 10–30 meV. We also found that the total energy is nearly independent of the choice of the smearing parameter σ, provided it is not too large ($\sigma \leqslant 0.05$ eV). Values from $\sigma = 0.01$ to 0.1 eV have been checked. Therefore we judge that our set of standard parameters ($E_{\max} = 268$ eV, supercell size a from 10 to 22 Å, and $\sigma = 0.02$ eV) offers a sufficiently good accuracy at a reasonable computational costs.

[37]M. Muñoz-Navia, J. Dorantes-Dávila, D. Zitoun, C. Amiens, B. Chaudret, M.-J. Casanove, P. Lecante, N. Jaouen, A. Rogalev, M. Respaud, and G. M. Pastor, Faraday Discuss. **138**, 181 (2008); M. Muñoz-Navia, J. Dorantes-Dávila, M. Respaud, and G. M. Pastor, Eur. Phys. J. D **52**, 171 (2009).

[38]G. M. Pastor, R. Hirsch, and B. Mühlschlegel, Phys. Rev. Lett. **72**, 3879 (1994); Phys. Rev. B **53**, 10382 (1996).

[39]R. Garibay-Alonso, J. Dorantes-Dávila, and G. M. Pastor, Phys. Rev. B **79**, 134401 (2009).

[40]Results for lower-lying isomers and excited magnetic configurations will be reported elsewhere.

[41]Y. Wang, T. F. George, D. M. Lindsay, and A. C. Beri, J. Chem. Phys. **86**, 3493 (1987).

[42]The precise choice of the NN distances is not very important, since this concerns merely the configuration for starting the unconstrained structural relaxation.

[43]G. Kresse and Jürgen Furthmüller, VASP *The Guide*, [http://cms.mpi.univie.ac.at/vasp].

[44]For a discussion of the interplay between electron correlations, structure, and magnetism of small clusters see, for example, Refs. 18 and 38.

[45]R. F. W. Bader, *Atoms in Molecules: A Quantum Theory* (Oxford University Press, Oxford, 1990).

[46]J. L. Ricardo-Chávez, PhD Thesis, Université Paul Sabatier, Toulouse, France, 2007.

[47]Y.-C. Bae, V. Kumar, H. Osanai, and Y. Kawazoe, Phys. Rev. B **72**, 125427 (2005).

[48]M. Muñoz-Navia, J. Dorantes-Dávila, D. Zitoun, C. Amiens, N. Jaouen, A. Rogalev, M. Respaud, and G. M. Pastor, Appl. Phys. Lett. **95**, 233107 (2009).